Chapter 10
A Method for the Quantification of Architectural Anisotropy in Cancellous Bone Samples Using CT Images

Nicolas Rogalski, Christophe Cluzel, and Sébastien Laporte

Abstract In osteoporotic patients, the sites most prone to fracture are characterized by a predominance of cancellous bone. It has been shown that trabecular architecture plays a crucial role in the mechanical performance of this type of bone. It therefore appears necessary to be able to describe this architecture within an elementary volume. This requires a quantification of the anisotropy of the bone, i.e. a description of the preferred orientations of its architectural elements. Classical techniques are based on the use of a symmetrical second-order tensor, implying orthotropic symmetry within the bone, which is not always the case. In order to properly characterize the architectural anisotropy of cancellous bone samples, this paper presents a new approach for computing the preferred orientations of CT-scanned samples. This method is based on the skeletonization of surfaces reconstructed from binarized CT images, on the use of a projector on the directing vectors of the skeletal rods and finally on the 3D surface analysis of the distribution of the orientations and lengths of the rods. The method introduced has made it possible to obtain the preferred directions of 52 samples of bovine cancellous bone and to show that, in general, these directions are not orthogonal, refuting the oversimplification of orthotropic models.

Keywords: Cancellous bone · Anisotropy · CT images

N. Rogalski, S. Laporte
Arts et Metiers Institute of Technology, Université Sorbonne Paris Nord, IBHGC - Institut de Biomécanique Humaine Georges Charpak, F-75013 Paris, France
e-mail: nicolas.rogalski@ensam.eu, sebastien.laporte@ensam.eu

C. Cluzel
Laboratoire de Mécanique et Technologie, Ecole Normale Supérieure Paris Saclay, Cachan, France
Département Science et Genie des Materiaux, Institut Universitaire de Technologie d'Evry Vald'Essonne, Every, France
e-mail: christophe.cluzel@ens-paris-saclay.fr

B. E. Abali and I. Giorgio (eds.), *Developments and Novel Approaches in Biomechanics and Metamaterials*, Advanced Structured Materials 132,
https://doi.org/10.1007/978-3-030-50464-9_10

10.1 Introduction

In osteoporosis, the sites most prone to fracture, whether hip, femur or vertebrae, are bone regions characterized by a predominance of cancellous bone (Liu et al, 2006). Cancellous bone plays a crucial role in charge transmission and energy absorption (Silva et al, 1997). However, despite the relationship between an increased risk of fracture and a decrease in bone mineral density (Cummings et al, 1993), more than half of postmenopausal women who have had a hip fracture have a density above the World Health Organization osteoporosis threshold (Wainwright et al, 2005). On the other hand, a study on microarchitectural differences between white women and Chinese American women showed that despite a lower bone mineral density, Chinese American women have fewer fractures than white women (Liu et al, 2011). The study of trabecular microstructure therefore contributes to the understanding of lesion mechanisms and the prediction of fracture risk.

To perform the mechanical study of trabecular microstructure, finite element calculations are currently used (Pottecher et al, 2016). However, these models do not integrate the microarchitectural specificities of trabecular bone. Another approach is to quantify the structural and mechanical anisotropy of bone (Gomez-Benito et al, 2005). Current methods allow to determine a symmetric, positive definite, second-rank fabric tensor, from which can be extracted estimates of principal component directions and magnitudes (Moreno et al, 2014) (the Mean Interception Length (MIL) (Whitehouse, 1974), the Volume Orientation (VO) (Odgaard et al, 1990), the Star Length Distribution (SLD) (Smit et al, 1998)). Although a second-rank tensor provides accurate information about a continuum material, it defines three orthogonal axes whereas the alignment directions of the elements of the trabecular network are not necessarily orthogonal (Ketcham and Ryan, 2004). It can also mask the secondary reinforcing directions, leading to an oversimplification in the case of porous materials such as trabecular bone.

The objective of this paper is therefore to introduce a method allowing the characterization of architectural anisotropy of cancellous bone samples from micro-scanner images in order to obtain the privileged orientations, but also to address the gaps among the various parameters described in the literature, used to analyze the microarchitecture of cancellous bone (Bouxsein et al, 2010); none provides information, at the scale of a representative elementary volume, on the directions of trabecular networks. The proposed tool is based on an analysis of three-dimensional geometric anisotropy in terms of trabecular orientation.

10.2 Material and Methods

10.2.1 Trabecular Bone Image Processing

The use of a CT-scan (Phoenix v | Tome | x L240 / NF180: 70 kV, 350 μA, acquisition time of 500 ms per image, resolution of 80 μm), allowed the acquisition of 2D images of cancellous bone. These images were binarized using a multi-level Otsu method (Otsu, 1979) (see Fig. 10.1). Using a segmentation algorithm, the 3D surfaces of the bone samples were obtained. Finally, a thinning algorithm (Lee et al, 1994) was used to skeletonize the surface.

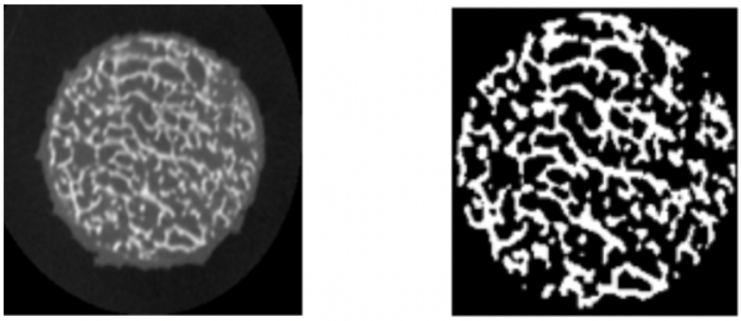

Fig. 10.1 2D Image from the CT-scan (left) and binarized image (right).

The curved lines of the skeleton were approximated by their chord to obtain a network of straight lines (see Fig. 10.2).

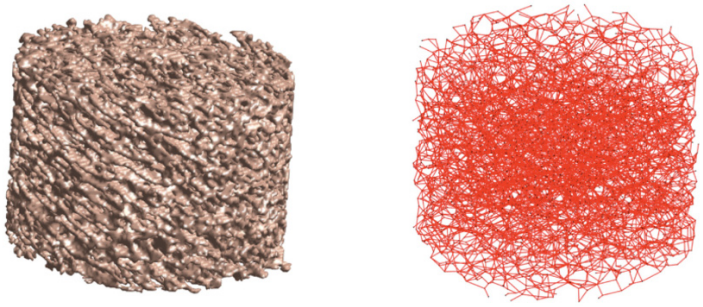

Fig. 10.2 Reconstructed surface (left) and sample after skeletonization (right).

10.2.2 The Projector

To analyze the architectural anisotropy of the samples in order to obtain the preferred alignment directions of the rods, as well as to obtain the distribution of their average lengths, a projector was introduced. The purpose of the projector, defined by equation (15.1), is to account for the relative contributions of rods of different orientations using their respective directing vectors. It takes the form:

$$k(\alpha_T, \alpha_0, p) = A\left(1 - e^{-\left(\frac{\pi - 2\alpha_T}{\pi - 2\alpha_0}\right)^p}\right) \tag{10.1}$$

- α_T: angle between the direction of interest and the mechanical axis of the trabeculae (radians).
- α_0: angular width of the projector (radians).
- p: power of the projector.

The principle is that of a filter: a direction of interest is first chosen. Then, if the angle between the axis (the directing vector) of a trabecula and the direction of interest is between 0 and α_0, the axis is projected on the direction of interest. This allows to group the similar contributions of orientation together in order to highlight the privileged directions. The p-factor provides better filtration quality. When p increases, the projector values for angles greater than α_0 tend towards 0 (see Fig. 10.3). It is therefore a question of finding a compromise between precision, relevance in the choice of secondary directions and calculation time.

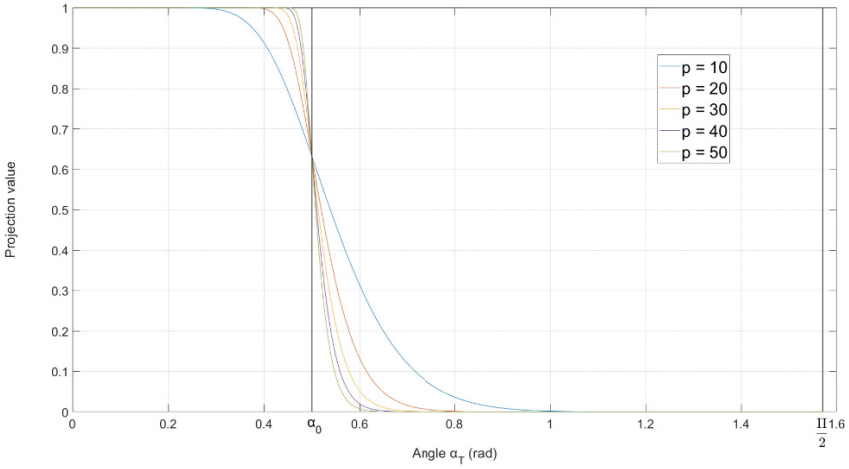

Fig. 10.3 Projector values as a function of angle α_T for different values of p.

From the projector, the 3D distribution of the trabeculae in the direction n is given by equation (15.2)

$$d_n(\alpha_0, p) = \frac{1}{N_{Trab}} \sum_{T=1}^{N_{Trab}} k(\alpha_T, \alpha_0, p) \tag{10.2}$$

The mean length of the trabeculae in the direction n is given by equation (15.3)

$$L_n(\alpha_0, p) = \frac{\sum_{T=1}^{N_{Trab}} L_T \, k(\alpha_T, \alpha_0, p)}{\sum_{T=1}^{N_{Trab}} k(\alpha_T, \alpha_0, p)} \tag{10.3}$$

Using the principle of 3D histogram on a continuous surface (cubed sphere Bruno, 2020) and the projector, it was possible to obtain 3D representations of the distribution of the orientations of the directing vectors of the rods as well as their lengths. The preferred orientations and rod lengths were then computed by analyzing the local extrema of the surfaces obtained, the low extrema being neglected. Finally, the samples were classified according to their number of preferred orientations.

10.2.3 Samples of Cancellous Bone

The image processing method and then the projector were used on cancellous bone samples from cattle aged about 4 years. 52 cylindrical samples (height: 7.5 mm, diameter: 10.5 mm) from the femoral head and greater trochanter of 6 different femurs were collected in collaboration with the BISRU laboratory at the University of Cape Town, South Africa (Prot, 2015) and processed.

10.3 Results

10.3.1 Influence of Projector Parameters

It is possible to play with the projector parameters (angular width and power) in order to monitor the effects of the filtration process and thus modify the shape of the 3D distribution of orientations. Decreasing the width allows to take into account privileged directions closer to each other and vice-versa. The parameter p is used to control the quality of filtration : it is possible to switch from binary filtration with a high power (the directing vector of the rod is included in the angular opening around the direction of interest, or not) to a softer filtration, for a lower power (see Fig. 10.3, 10.4).

The principle is the same for the distribution of lengths (see Fig. 10.5).

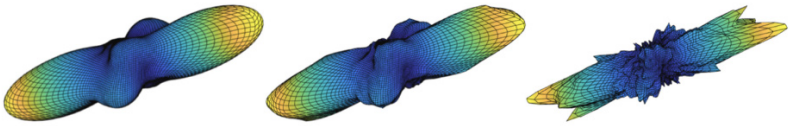

Fig. 10.4 Influence of the projector parameters on the 3D distribution of the rod orientations. (a): α_0=10°, p=20 (b): α_0=2°, p=20 (c): α_0=2°, p=40.

10.3.2 Use of the Projector on Bone Samples

By using the projector on bone samples treated with the method described in 10.2.1 and computing the local extrema of the resulting surface, the preferred orientations, the mean rod lengths, the rod length standard deviations and the mean angles between the directing vectors of the preferred orientations were obtained. The samples were sorted in three groups according to their number of preferred orientations (Table 15.1, 15.2).

Table 10.1 Mean trabecular lengths, length standard deviations for the different groups of cancellous bone samples.

Number of preferred orientations	Mean trabecular length (μm)	Length standard deviation (μm)
4	484.72	13.89
3	476.77	11.29
2	476.54	13.98

Five samples were not referenced because the number of orientations was greater than 4. In this case, the relative importance of the orientations within the network decreases as the bone approaches the isotropic case, which makes their determination more difficult. Fig. 10.6 illustrates the different possible configurations within the samples, in terms of preferred orientations.

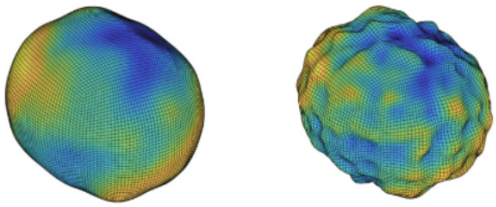

Fig. 10.5 Influence of the projector parameters on the 3D distribution of rod lengths. (a): α_0=10°, p=20, (b): α_0=5°, p=40.

Table 10.2 Mean angles between the directing vectors of preferred orientations for the different groups of cancellous bone samples. Angles of directing vectors (deg).

Number of preferred orientations	$(\widehat{\mathbf{v_1}\mathbf{v_2}})$	$(\widehat{\mathbf{v_1}\mathbf{v_3}})$	$(\widehat{\mathbf{v_2}\mathbf{v_3}})$	$(\widehat{\mathbf{v_1}\mathbf{v_4}})$	$(\widehat{\mathbf{v_2}\mathbf{v_4}})$	$(\widehat{\mathbf{v_3}\mathbf{v_4}})$
4	60.03	79.02	64.96	66.26	75.89	53.38
3	72.95	72.76	76.6			
2	74.42					

10.4 Discussion

In this paper, an approach allowing the quantification of architectural anisotropy as well as obtaining information on the average length of rods in a sample of cancellous bone was presented. The method relies on the use of a set of images acquired by a CT-scan, processed to reconstruct a surface and a tool based on the principle of projection of the directing vectors of the rods after skeletonization of the surface.

The projector offers the possibility of computing non-orthogonal privileged directions and secondary directions, contrary to conventional techniques for quantifying architectural anisotropy, such as the MIL, the VO or the SLD. It has been shown that the measured angles between the preferred directions are on average quite far apart from 90 degrees (Table 15.2), which proves that the hypothesis of orthotropy within the trabecular network is over-simplifying in most cases. Highlighting the actual preferred directions is essential because the mechanics of cancellous bone is driven by its microstructure.

The whole approach presents some drawbacks though. In particular, the method presents a sensitivity due to the imaging techniques used. The resolution of the scan must be sufficient to preserve a maximum of information on the architecture of the

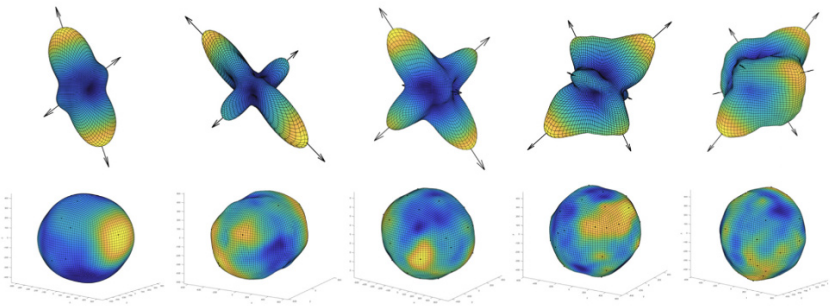

Fig. 10.6 3D distribution of orientations and trabecular length (in μm) for bone samples (α_0=10°, p=20). From left to right: 2 non-orthogonal orientations, 2 orthogonal orientations, 3 orthogonal orientations, 3 non-orthogonal orientations, 4 orientations.

bone, but the possibility of clinical use must also be taken into account, which limits the minimum usable resolution. Moreover, the resolution also affects the choice of the projector parameters. Indeed, the chosen voxel size allows to obtain a minimum angular width value below which one cannot work, this value corresponding to the positioning inaccuracy of the bone sample in the scanner (see Fig. 10.7).

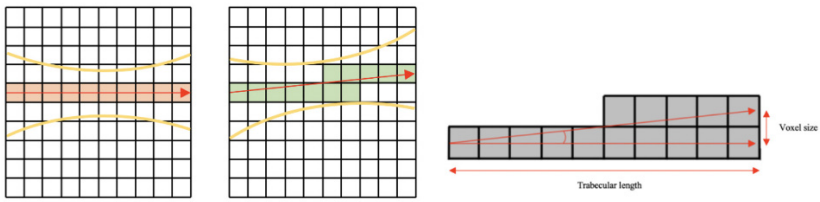

Fig. 10.7 Difference in rod orientation obtained after skeletonization by considering the positioning uncertainty in the CT-scan.

Considering an average rod length of $480\ \mu m$ (see Table 15.1) as well as a voxel size of $80\ \mu m$, the angle corresponding to this uncertainty equals approximately 9.5 degrees. The voxel size therefore limits the angular width of the projector.

In addition, the thinning algorithm used does not differentiate the plate and rods elements of the samples. The skeleton shows only rods. A more complex algorithm can be used to preserve this distinction in the skeletonization process, as it was shown that plates play a crucial role in the mechanical behavior of cancellous bone in several regions of the body (Wang et al, 2013). Another point is that the rods are approximated by their chord, their curves are neglected. It is advisable to take this into account later on, in order to obtain a more accurate geometric description and to be able to envisage damage phenomena linked to microarchitecture (buckling for example). Finally, the application of this tool will be more difficult to implement than the above-mentioned techniques because it will rely on the use of higher order tensors, in order to be able to use all the geometrical information obtained from the projector.

Once the improvements listed have been incorporated, it will then be possible to compare the method presented to other methods that do not rely on a skeletonization process, such as the use of facet normals of a STL file (Cluzel and Allena, 2018). It would also be interesting to carry out a mapping of the anisotropic field of coordinates on the femurs where the samples were taken, similarly to the work done on cortical bone for orthotropic directions (Allena and Cluzel, 2018). This would allow to show the alignment of the privileged orientations with the mechanical loading axes, which would constitute a validation of the interest of the approach based on physiology. A method allowing the detection of extrema based on the norm of orientation vectors could be considered in order to automatically neglect low intensity directions within the network.

References

Allena R, Cluzel C (2018) Heterogeneous directions of orthotropy in three-dimensional structures: finite element description based on diffusion equations. Mathematics and Mechanics of Complex Systems 6(4):339–351

Bouxsein ML, Boyd SK, Christiansen BA, Guldberg RE, Jepsen KJ, Müller R (2010) Guidelines for assessment of bone microstructure in rodents using micro-computed tomography. Journal of Bone and Mineral Research: The Official Journal of the American Society for Bone and Mineral Research 25(7):1468–1486

Bruno L (2020) Cubed Sphere

Cluzel C, Allena R (2018) A general method for the determination of the local orthotropic directions of heterogeneous materials: application to bone structures using μCT images. Mathematics and mechanics of complex systems 6(4):353–367

Cummings SR, Browner W, Cummings SR, Black DM, Nevitt MC, Browner W, Genant HK, Cauley J, Ensrud K, Scott J, Vogt TM (1993) Bone density at various sites for prediction of hip fractures. The Lancet 341(8837):72–75

Gomez-Benito MJ, Garcıa-Aznar JM, Doblare M (2005) Finite Element Prediction of Proximal Femoral Fracture Patterns Under Different Loads. Journal of Biomechanical Engineering 127(1):9–14

Ketcham RA, Ryan TM (2004) Quantification and visualization of anisotropy in trabecular bone. Journal of Microscopy 213(2):158–171

Lee TC, Kashyap RL, Chu CN (1994) Building Skeleton Models via 3-D Medial Surface Axis Thinning Algorithms. CVGIP: Graphical Models and Image Processing 56(6):462–478

Liu XS, Sajda P, Saha PK, Wehrli FW, Guo XE (2006) Quantification of the Roles of Trabecular Microarchitecture and Trabecular Type in Determining the Elastic Modulus of Human Trabecular Bone. Journal of bone and mineral research : the official journal of the American Society for Bone and Mineral Research 21(10):1608–1617

Liu XS, Walker MD, McMahon DJ, Udesky J, Liu G, Bilezikian JP, Guo XE (2011) Better skeletal microstructure confers greater mechanical advantages in Chinese-American women versus white women. Journal of Bone and Mineral Research: The Official Journal of the American Society for Bone and Mineral Research 26(8):1783–1792

Moreno R, Borga M, Smedby O (2014) Techniques for Computing Fabric Tensors: A Review. In: Westin CF, Vilanova A, Burgeth B (eds) Visualization and Processing of Tensors and Higher Order Descriptors for Multi-Valued Data, Springer, Berlin, Heidelberg, Mathematics and Visualization, pp 271–292

Odgaard A, Jensen EB, Gundersen HJG (1990) Estimation of structural anisotropy based on volume orientation. A new concept. Journal of Microscopy 157(2):149–162

Otsu N (1979) A Threshold Selection Method from Gray-Level Histograms. IEEE Transactions on Systems, Man, and Cybernetics 9(1):62–66

Pottecher P, Engelke K, Duchemin L, Museyko O, Moser T, Mitton D, Vicaut E, Adams J, Skalli W, Laredo JD, Bousson V (2016) Prediction of Hip Failure Load: In Vitro Study of 80 Femurs Using Three Imaging Methods and Finite Element Models-The European Fracture Study (EFFECT). Radiology 280(3):837–847

Prot M (2015) Comportement mécanique de l'os spongieux à différentes vitesses de déformation. : relations entre architecture et réponse mécanique. thesis, Paris, ENSAM

Silva MJ, Keaveny TM, Hayes WC (1997) Load sharing between the shell and centrum in the lumbar vertebral body. Spine 22(2):140–150

Smit, Schneider, Odgaard (1998) Star length distribution: a volume-based concept for the characterization of structural anisotropy. Journal of Microscopy 191(3):249–257

Wainwright SA, Marshall LM, Ensrud KE, Cauley JA, Black DM, Hillier TA, Hochberg MC, Vogt MT, Orwoll ES, Study of Osteoporotic Fractures Research Group (2005) Hip fracture in women without osteoporosis. The Journal of Clinical Endocrinology and Metabolism 90(5):2787–2793

Wang J, Zhou B, Parkinson I, Thomas CDL, Clement JG, Fazzalari N, Guo XE (2013) Trabecular Plate Loss and Deteriorating Elastic Modulus of Femoral Trabecular Bone in Intertrochanteric Hip Fractures. Bone Research 1(1):346–354

Whitehouse WJ (1974) The quantitative morphology of anisotropic trabecular bone. Journal of Microscopy 101(Pt 2):153–168